

# Pareto Control Barrier Function for Inner Safe Set Maximization Under Input Constraints

Xiaoyang Cao<sup>1</sup>, Zhe Fu<sup>2,\*</sup> and Alexandre M. Bayen<sup>2</sup>

**Abstract**— This article introduces the Pareto Control Barrier Function (PCBF) algorithm to maximize the inner safe set of dynamical systems under input constraints. Traditional Control Barrier Functions (CBFs) ensure safety by maintaining system trajectories within a safe set but often fail to account for realistic input constraints. To address this problem, we leverage the Pareto multi-task learning framework to balance competing objectives of safety and safe set volume. The PCBF algorithm is applicable to high-dimensional systems and is computationally efficient. We validate its effectiveness through comparison with Hamilton-Jacobi reachability for an inverted pendulum and through simulations on a 12-dimensional quadrotor system. Results show that the PCBF consistently outperforms existing methods, yielding larger safe sets and ensuring safety under input constraints.

## I. INTRODUCTION

Control Barrier Functions (CBFs) provide a powerful method to ensure the safety of autonomous systems by maintaining system trajectories within a predefined safe set [1]. They have been successfully applied in various domains, including robotics [2] and autonomous vehicles [3].

However, ensuring safety becomes challenging when systems operate under input constraints [4]–[7]. Traditional CBFs typically assume the availability of arbitrary control inputs [8], [9], which allows the system to be guided within the safe set without limitations. However, this assumption often overlooks the practical reality that control inputs are constrained by physical limitations of actuators, energy resources, or other system-specific constraints. As a result, the safe set may no longer be forward invariant under such restricted inputs [4].

**CBFs under input constraints:** Recent research has tried to address this problem. Agrawal and Panagou [4] introduced Input Constrained CBFs (ICCBFs), iteratively defining functions to form an inner safe set  $C^*$  that is forward invariant under input constraints. Breeden and Panagou [5] introduced Zeroing CBFs (ZCBFs) for high-relative-degree systems, ensuring forward invariance by converting higher-order constraints into ZCBFs. However, both approaches tend to be overly conservative, as they do not guarantee the largest possible safe set, potentially limiting the system’s operational flexibility.

**Neural CBFs:** Neural CBFs (NCBFs) have emerged as an effective approach for ensuring safety in complex, high-dimensional systems, where traditional CBFs may be difficult to design [10]. These methods have been extended to handle

parametric uncertainties, unknown dynamic environments, and safe navigation tasks [11]–[13]. However, few works have integrated input constraints into NCBFs. Liu et al. proposed the non-saturating CBF (NSCBF) to handle input constraints solving a min-max optimization [6]. Though effective, the complexity of this approach leads to longer training times. Oswin et al. introduced a policy NCBF based on policy iteration [7]. However, their method doesn’t guarantee the largest possible inner safe set either.

**HJ reachability:** Hamilton-Jacobi (HJ) reachability analysis theoretically computes the largest control-invariant set [14]. Recent work has combined HJ reachability with CBFs to mitigate the overly conservative problem of HJ policies [15]. However, HJ reachability is computationally intensive and practically limited to systems with fewer than five dimensions, restricting its applicability in higher-dimensional dynamical systems.

We summarize our contributions as follows:

- **Maximizing Inner Safe Set:** We propose the PCBF algorithm (Algorithm 1) to determine the largest inner safe set under input constraints.
- **Reduced Training Time:** We enhance training efficiency by applying a Gaussian sampling method to the inner safe set’s interior.
- **Validation on Benchmark Systems:** We validate our method by comparing PCBF results for the inverted pendulum with HJ reachability and through simulations on a 12-dimensional quadrotor system.

The remainder of this article is organized as follows: Section II provides preliminaries, including problem definition, CBFs, Neural CBFs, and Pareto Multi-task Learning. Section III presents our methodology, detailing the PCBF algorithm. Section IV demonstrates the effectiveness of our approach through experiments on an inverted pendulum and a quadrotor system. Finally, Section V concludes the paper and discusses future work directions.

## II. PRELIMINARIES

### A. Problem Definition

We consider continuous-time, control-affine dynamics:

$$\dot{x} = f(x) + g(x)u, \quad (1)$$

where  $x \in \mathcal{X} \subseteq \mathbb{R}^n$ ,  $u \in \mathcal{U} \subseteq \mathbb{R}^m$ , and  $f, g$  are locally Lipschitz continuous functions. To ensure safety, we introduce the concept of a safe set.

\*Corresponding author. Email: zhefu@berkeley.edu

<sup>1</sup>Tsinghua University, Beijing, China

<sup>2</sup>University of California, Berkeley, CA, USA

**Definition 1** (Safe Set). *The Safe Set  $S$  is defined as:*

$$S \triangleq \{x \in \mathcal{X} : h(x) \geq 0\}, \quad (2)$$

where  $h : \mathcal{X} \rightarrow \mathbb{R}$  is a continuously differentiable function.

The safe set  $S$  is defined to include all states  $x$  in which the system remains safe during operation. In practice, the safe set often comes from the physical constraints and safety requirements inherent in the system, such as avoiding collisions or maintaining stability. However, due to the presence of input constraints, ensuring forward invariance of the entire safe set is challenging [4]. Thus, the concept of an inner safe set is introduced.

**Definition 2** (Forward Invariant). *A set  $C \subseteq \mathbb{R}^n$  is forward invariant under a dynamical system (1) if for any initial condition  $x(0) \in C$ , the trajectory  $x(t) \in C$  for all  $t \geq 0$ .*

**Definition 3** (Inner Safe Set [4]). *An Inner Safe Set  $C$  is a non-empty, closed subset of the safe set  $S$  such that there exists a feedback controller  $\pi : C \rightarrow \mathcal{U}$  that renders  $C$  forward invariant under the system dynamics.*

The goal of this research is to find the largest such inner safe set given the system's input constraints. The problem is formulated as below:

**Problem 1** (Inner Safe Set Maximization). *Given a dynamical system (1) and a safe set  $S \subseteq \mathcal{X}$ , determine the largest possible inner safe set  $C^* \subseteq S$  and a control policy  $\pi : C^* \rightarrow \mathcal{U}$  such that  $C^*$  remains forward invariant under the system dynamics.*

### B. Control Barrier Functions

**Definition 4** (Control Barrier Functions (CBFs)). *A function  $h : \mathcal{X} \rightarrow \mathbb{R}$  is considered a CBF if there exists an extended class- $\mathcal{K}$  function <sup>1</sup>  $\alpha$  such that for all states  $x \in \mathcal{X}$ , the following inequality holds:*

$$\sup_{u \in \mathcal{U}} [L_f h(x) + L_g h(x)u] \geq -\alpha(h(x)), \quad (3)$$

where  $L_f h(x) = \nabla h(x)^\top f(x)$  and  $L_g h(x) = \nabla h(x)^\top g(x)$  are the Lie derivatives of  $h(x)$  along the vector fields  $f(x)$  and  $g(x)$ , respectively.

CBFs provide a systematic approach to ensuring the forward invariance of safe sets by applying the following lemma [1]:

**Lemma 1** (Ames et al. [1]). *Given a set  $C = \{x \in \mathcal{X} : h(x) \geq 0\}$  defined by a CBF  $h(x)$ , the set  $C$  is forward invariant under the control input  $u \in \mathcal{U}$  if there exists a feedback controller  $\pi(x)$  such that:*

$$L_f h(x) + L_g h(x)\pi(x) \geq -\alpha(h(x)), \quad \forall x \in C. \quad (4)$$

The CBF Quadratic Program (CBF-QP) is formulated to find the optimal control input  $u(x)$  that minimizes the

deviation from the desired control  $u_{\text{des}}$  while satisfying the CBF's safety constraints:

**Problem 2** (CBF-QP).

$$\begin{aligned} \min_{u \in \mathcal{U}} \quad & \|u - u_{\text{des}}(x)\|^2 \\ \text{s.t.} \quad & L_f h(x) + L_g h(x)u \geq -\alpha(h(x)). \end{aligned} \quad (5)$$

**Justification for the need of an inner safe set:** When  $\mathcal{U}$  is unbounded, since (3) is linear in  $u$ , it is always possible to find a valid CBF and corresponding control input  $u$  satisfying (3) if  $L_g h(x) \neq 0$ .

However, when input constraints exist, the control input  $u$  satisfying (3) may not always comply with the constraints. Certain states within the safe set may no longer be forward invariant. Therefore, the challenge becomes identifying the largest subset of the safe set, the maximum inner safe set.

### C. Neural CBFs

NCBFs address the difficulty of hand-designing CBFs for complex systems by using neural networks to approximate a valid CBF  $h_{\theta_1}(x)$  and its corresponding controller  $\pi_{\theta_2}(x)$ , where  $\theta_1$  and  $\theta_2$  are the parameters of the neural networks for the CBF and controller, respectively [10], [16]. For a given safe set  $\mathcal{S}$ , NCBFs define three loss functions:  $\mathcal{L}_{\text{safe}}$ ,  $\mathcal{L}_{\text{unsafe}}$ , and  $\mathcal{L}_{\text{feas}}$ . To compute these losses, we sample a set of points  $\mathbb{X} = \{x_1, \dots, x_N\} \subset \mathcal{X}$ , where  $N$  is the number of sampled points. Let  $N_{\text{safe}}$  and  $N_{\text{unsafe}}$  denote the number of sampled points from the safe set  $\mathcal{S}$  and the complement of the safe set  $\mathcal{X} \setminus \mathcal{S}$ .

$$\mathcal{L}_{\text{safe}} = \frac{1}{N_{\text{safe}}} \sum_{x_i \in \mathbb{X} \cap \mathcal{S}} \max\{0, -h_{\theta_1}(x_i)\}, \quad (6)$$

$$\mathcal{L}_{\text{unsafe}} = \frac{1}{N_{\text{unsafe}}} \sum_{x_i \in \mathbb{X} \cap (\mathcal{X} \setminus \mathcal{S})} \max\{0, h_{\theta_1}(x_i)\}, \quad (7)$$

$$\mathcal{L}_{\text{feas}} = \frac{1}{N_{\text{safe}}} \sum_{x_i \in \mathbb{X} \cap \mathcal{S}} \max\{0, -[L_f h_{\theta_1}(x_i) + L_g h_{\theta_1}(x_i)\pi_{\theta_2}(x_i) + \alpha(h_{\theta_1}(x_i))]\}. \quad (8)$$

$\mathcal{L}_{\text{safe}}$  and  $\mathcal{L}_{\text{unsafe}}$  penalize states where  $h_{\theta_1}(x)$  misclassifies safety, either within the safe set or outside it, while  $\mathcal{L}_{\text{feas}}$  ensures  $\pi_{\theta_2}(x)$  satisfies the feasibility condition (4) for forward invariance.

However, such NCBFs still require a predefined safe set. Liu et al. [6] proposed the NSCBF  $h_\theta(x)$ , which removes the need for a predefined safe set and directly handles input constraints:

$$h_\theta(x) = h(x) - (\text{nn}_\theta(x) - \text{nn}_\theta(x_e))^2, \quad (9)$$

where  $\text{nn}_\theta(x)$  is a neural network with parameter  $\theta \in \mathbb{R}^p$ , and  $x_e$  is a known safe state that must be included in the learned inner safe set. Typically, in problems aimed at maintaining the system's proximity to a stable point,  $x_e$  is the stable point itself. For obstacle avoidance problems,  $x_e$  can be a point far

<sup>1</sup>An extended class- $\mathcal{K}$  function is a strictly increasing, continuous function  $\alpha : \mathbb{R} \rightarrow \mathbb{R}$  with  $\alpha(0) = 0$ .

from the obstacle. This method ensures that the learned inner safe set  $C_{h_\theta} = \{x \in \mathcal{X} : h_\theta(x) \geq 0\}$  is always a subset of the original safe set. Also,  $C_{h_\theta}$  is always a non-empty set, guaranteeing that there are sufficient sample points during the training process.

Ensuring that the learned inner safe set satisfies input constraints, Liu et al. [6] calculate the saturation risk by evaluating the worst-case violation of safety constraints along the boundary of  $C_{h_\theta}$ . To increase the volume of the inner safe set, a regularization term is introduced to encourage the expansion of the safe set. Finally, the total loss is a linear combination of the saturation risk and the regularization term.

Although this method has shown success in specific cases, it has several limitations. First, sampling on  $\partial C_{h_\theta}$  to calculate the saturation risk is computationally expensive; second, the regularization term does not guarantee finding the largest possible safe set. Even for the maximal inner safe set, the regularization term remains non-zero, which can lead to suboptimal solutions.

### III. METHODOLOGY

We introduce the Pareto multi-task learning framework [17] into traditional NCBFs to propose the PCBF algorithm. This approach achieves a balance between ensuring safety and maximizing the inner safe set under input constraints. We use the NCBF formulation from equation (9) in this study.

#### A. Loss Function Design

Our loss function consists of two main components: the feasibility loss and the volume loss. Computing these two losses require sampling in the state space. To ensure sufficient data density near the known safe state  $x_e \in \mathcal{X}$ , we employ a multivariate Gaussian sampling method  $\mathbb{X}_{\mathcal{N}} = \{x_i \mid x_i \stackrel{\text{i.i.d.}}{\sim} \mathcal{N}(x_e, \Sigma), i = 1, 2, \dots, N_{\mathcal{N}}\} \subset \mathcal{X}$ , where  $N_{\mathcal{N}}$  is the number of sampled points. The covariance matrix  $\Sigma$  is diagonal, with each diagonal element defined as  $\sigma_{ii} = \frac{\Delta x_i}{k}$ , where  $\Delta x_i$  is the state space length in the  $i$ -th dimension, and  $k$  is a positive hyperparameter. The feasibility loss  $\mathcal{L}_{\text{feas}}$  ensures that the learned inner safe set  $C_{h_\theta}$  is forward invariant:

$$\mathcal{L}_{\text{feas}} = \frac{1}{N_{\mathcal{N}}} \sum_{x_i \in \mathbb{X}_{\mathcal{N}} \cap C_{h_\theta}} \max\{0, -\sup_{u \in \mathcal{U}} \phi_\theta(x_i, u)\}, \quad (10)$$

$$\phi_\theta(x, u) = L_f h_\theta(x) + L_g h_\theta(x)u + \alpha(h_\theta(x)), \quad (11)$$

For simplicity, we assume linear input constraints, making  $\mathcal{U}$  a polyhedron. Since  $\phi_\theta(x, u)$  is affine in  $u$ , the supremum over  $\mathcal{U}$  is necessarily achieved at some vertex of  $\mathcal{U}$ , allowing closed-form computation of  $\mathcal{L}_{\text{feas}}$ .

$$\sup_{u \in \mathcal{U}} \phi_\theta(x, u) = \max_{u \in \mathcal{V}(\mathcal{U})} \phi_\theta(x, u), \quad (12)$$

where  $\mathcal{V}(\mathcal{U})$  is the set of vertexes of  $\mathcal{U}$ . The volume loss  $\mathcal{L}_{\text{vol}}$  is designed to encourage the expansion of the learned inner safe set by minimizing the deviation from  $\mathcal{S}$ :

$$\mathcal{L}_{\text{vol}} = \frac{1}{N_{\mathcal{N}}} \sum_{x_i \in \mathbb{X}_{\mathcal{N}} \cap C_{h_\theta}} (\text{nn}_\theta(x_i) - \text{nn}_\theta(x_e))^2, \quad (13)$$

However, a simple linear combination of these loss functions does not guarantee a maximized inner safe set. The feasibility loss and the volume loss are inherently competing as both cannot be zero simultaneously—expanding the safe set violates safety constraints, and satisfying constraints reduces the set’s volume.

To address this challenge, the Pareto multi-task learning framework is introduced to balance these conflicting objectives.

#### B. Pareto Multi-task Learning (PMTL)

Consider  $M$  correlated tasks with a loss vector:

$$\mathbf{L}(\theta) = [\mathcal{L}_1(\theta) \quad \mathcal{L}_2(\theta) \quad \cdots \quad \mathcal{L}_M(\theta)]^T, \theta \in \mathbb{R}^p, \quad (14)$$

where  $\mathcal{L}_i(\theta)$  is the loss of the  $i$ -th task. In general, it is impossible to find a single solution  $\theta$  that simultaneously optimizes all the objectives. Instead, we can identify a collection of Pareto optimal solutions, each representing a distinct optimal trade-off among the various objectives [17].

**Definition 5** (Pareto Dominance). *A solution  $\theta$  dominates another solution  $\hat{\theta}$  if:*

- $\forall i \in \{1, \dots, M\}, \mathcal{L}_i(\theta) \leq \mathcal{L}_i(\hat{\theta})$ ,
- $\exists j \in \{1, \dots, M\}$  such that  $\mathcal{L}_j(\theta) < \mathcal{L}_j(\hat{\theta})$ .

**Definition 6** (Pareto Optimality). *A solution  $\theta$  is Pareto optimal if no other solution  $\hat{\theta}$  exists that dominates  $\theta$ .*

In other words, a solution  $\theta$  is considered Pareto optimal if no other feasible solution  $\hat{\theta}$  exists that can reduce any loss without simultaneously increasing at least one other loss.

**Definition 7** (Pareto Front). *The Pareto Front  $P_{\mathcal{L}}$  is the set of all loss vectors associated with the Pareto optimal solutions:*

$$P_{\mathcal{L}} = \{\mathbf{L}(\theta) \mid \theta \in \mathbb{R}^p \text{ is Pareto optimal}\}. \quad (15)$$

The Pareto front represents the best possible trade-offs among the competing objectives that can be achieved by any solution. PMTL provides a framework for simultaneously optimizing multiple objectives and converge to the Pareto front. Two common PMTL methods are:

**Linear combination:** A non-negative linear weighted sum is utilized to aggregate the losses of all tasks into a single loss:  $\mathcal{L}(\theta) = \sum_{i=1}^M \lambda_i \mathcal{L}_i(\theta)$ , where  $\lambda_i \geq 0$  is the weight for the  $i$ -th task. While straightforward, this approach has some limitations: firstly, selecting appropriate values for  $\lambda_i$  is challenging and often requires extensive empirical tuning; secondly, this method can only yield solutions on the convex portion of the Pareto front [18].

**Gradient-based method:** Fliege and Svaiter [19] proposed a gradient-based method generalizing the single objective steepest descent algorithm. The algorithm’s update rule is given by:  $\theta_{t+1} = \theta_t + \eta d_t$ , where  $\eta > 0$  is the learning

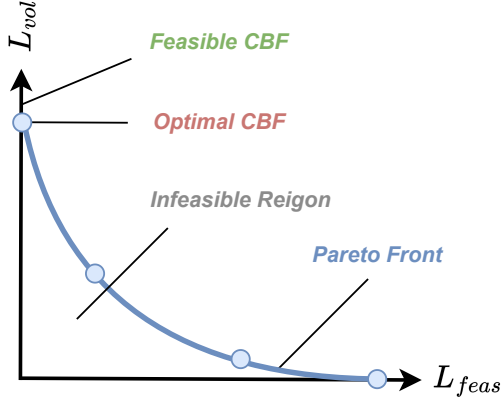


Fig. 1. Pareto front of the Inner Safe Set Maximization Problem. The blue line represents the Pareto front, which delineates the boundary between the feasible and infeasible regions in the objective space. No solution  $\theta$  can produce objective values  $[\mathcal{L}_{\text{feas}}(\theta), \mathcal{L}_{\text{vol}}(\theta)]^T$  that lie below this curve. The vertical axis represents solutions with zero feasibility loss. All feasible CBFs lie on this axis. The optimal CBF, with parameter  $\theta^*$ , lies at the intersection of the Pareto front and the vertical axis.

rate and the search direction  $d_t \in \mathbb{R}^p$  is obtained by solving following optimization problems:

$$(d_t, \alpha_t) = \arg \min_{d \in \mathbb{R}^p, \alpha \in \mathbb{R}} \alpha + \frac{1}{2} \|d\|^2 \quad (16)$$

$$\text{s.t. } \nabla \mathcal{L}_i(\theta_t)^T d \leq \alpha, \quad i = 1, \dots, M.$$

The solutions of this problem satisfy the following lemma:

**Lemma 2** (Fliege and Svaiter [19]). *Let  $(d_t, \alpha_t)$  be the solution of problem (16). Then:*

- 1) If  $\theta_t$  is Pareto critical, then  $d_t = 0 \in \mathbb{R}^p$  and  $\alpha_t = 0$ .
- 2) If  $\theta_t$  is not Pareto critical, then

$$\alpha_t \leq -\frac{1}{2} \|d_t\|^2 < 0, \quad (17)$$

$$\nabla \mathcal{L}_i(\theta_t)^T d_t \leq \alpha_t, \quad i = 1, \dots, M. \quad (18)$$

A solution  $\theta$  is said to be Pareto critical if there is no solution in its neighborhood can have better performance in all tasks. If  $\theta_t$  is Pareto critical,  $d_t = 0$  and  $\theta_t$  will not be updated. If  $\theta_t$  is not Pareto critical, then  $d_t$  is a descent direction for all tasks.

### C. Pareto Control Barrier Function (PCBF)

Problem 1 can be reformulated as a PMTL problem involving two competing objectives: volume loss  $\mathcal{L}_{\text{vol}}$  and feasibility loss  $\mathcal{L}_{\text{feas}}$ . The desired Pareto optimal solution, denoted as  $\theta^*$ , achieves zero feasibility loss while minimizing the volume loss:

**Problem 3** (Reformulation of Inner Safe Set Maximization).

$$\theta^* = \arg \min_{\theta \in \mathbb{R}^p} \mathcal{L}_{\text{vol}}(\theta) \quad (19)$$

$$\text{s.t. } \mathcal{L}_{\text{feas}}(\theta) = 0.$$

**Lemma 3.** *Let  $\theta^*$  be the solution to problem 3, then  $\theta^*$  is Pareto optimal, and the loss vector  $[\mathcal{L}_{\text{feas}}(\theta^*), \mathcal{L}_{\text{vol}}(\theta^*)]^T$  lies on the Pareto front.*

Lemma 3 establishes a direct connection between the inner safe set maximization problem 3 and the PMTL framework. Figure 1 illustrates the trade-offs between the two losses on the Pareto front.

The PCBF algorithm uses gradient-based multi-objective optimization methods to efficiently converge to the optimal parameter  $\theta^*$ . It has two main phases: initialization and parameter update.

- **Initialization:** The  $\text{nn}_{\theta}(\cdot)$  model in equation (9) is trained with a linear combination loss  $\mathcal{L}_{\text{lc}}(\theta_t) = \lambda_1 \mathcal{L}_{\text{feas}}(\theta_t) + \lambda_2 \mathcal{L}_{\text{vol}}(\theta_t)$  from a randomly initialized  $\theta_0 \in \mathbb{R}^p$ . Here  $\lambda_1, \lambda_2 \geq 0$  are hand-designed parameters. At each iteration  $t$ , parameters are updated by:  $\theta_{t+1} = \theta_t - \eta \nabla \mathcal{L}_{\text{lc}}(\theta_t)$ . This phase provides an initial solution close to  $\theta^*$  for further optimization.
- **Parameter update:** In this phase, the parameter  $\theta_t$  is updated iteratively by  $\theta_{t+1} = \theta_t + \eta d_t$ . The update direction  $d_t$  is determined by solving multiple instances of problem (16) with different loss configurations.

**Objective space decomposition:** As shown in Figure 2, in the parameter update phase, the objective space is partitioned into three regions using two parallel lines: the upper bound  $\mathcal{L}_{\text{vol}}(\theta) = \beta \mathcal{L}_{\text{feas}}(\theta) + \epsilon_{\text{ub}}$  and the lower bound  $\mathcal{L}_{\text{vol}}(\theta) = \beta \mathcal{L}_{\text{feas}}(\theta) + \epsilon_{\text{lb}}$ , where  $\beta$ ,  $\epsilon_{\text{ub}}$ , and  $\epsilon_{\text{lb}}$  are hyperparameters. The key idea of the PCBF is restricting the loss vector between these two bounds, where  $\theta^*$  is the solution to Problem 3, we impose<sup>2</sup> the constraints  $\beta > 0$  and  $0 \leq \epsilon_{\text{lb}} \leq \mathcal{L}_{\text{vol}}(\theta^*) \leq \epsilon_{\text{ub}}$ . For each region, we solve different subproblems to determine the update direction  $d_t$ :

- 1) If  $\mathcal{L}_{\text{vol}}(\theta_t) > \beta \mathcal{L}_{\text{feas}}(\theta_t) + \epsilon_{\text{ub}}$ :

$$(d_t, \alpha_t) = \arg \min_{d \in \mathbb{R}^p, \alpha \in \mathbb{R}} \alpha + \frac{1}{2} \|d\|_2^2 \quad (20)$$

$$\text{s.t. } [\nabla(\mathcal{L}_{\text{vol}}(\theta_t) - \beta \mathcal{L}_{\text{feas}}(\theta_t))]^T d \leq \alpha,$$

$$\nabla \mathcal{L}_{\text{feas}}(\theta_t)^T d \leq \alpha.$$

- 2) If  $\beta \mathcal{L}_{\text{feas}}(\theta_t) + \epsilon_{\text{lb}} \leq \mathcal{L}_{\text{vol}}(\theta_t) \leq \beta \mathcal{L}_{\text{feas}}(\theta_t) + \epsilon_{\text{ub}}$ :

$$(d_t, \alpha_t) = \arg \min_{d \in \mathbb{R}^p, \alpha \in \mathbb{R}} \alpha + \frac{1}{2} \|d\|_2^2 \quad (21)$$

$$\text{s.t. } \nabla \mathcal{L}_{\text{vol}}(\theta_t)^T d \leq \alpha,$$

$$\nabla \mathcal{L}_{\text{feas}}(\theta_t)^T d \leq \alpha.$$

- 3) If  $\mathcal{L}_{\text{vol}}(\theta_t) < \beta \mathcal{L}_{\text{feas}}(\theta_t) + \epsilon_{\text{lb}}$ :

$$(d_t, \alpha_t) = \arg \min_{d \in \mathbb{R}^p, \alpha \in \mathbb{R}} \alpha + \frac{1}{2} \|d\|_2^2 \quad (22)$$

$$\text{s.t. } [\nabla(\beta \mathcal{L}_{\text{feas}}(\theta_t) - \mathcal{L}_{\text{vol}}(\theta_t))]^T d \leq \alpha,$$

$$\nabla \mathcal{L}_{\text{feas}}(\theta_t)^T d \leq \alpha.$$

<sup>2</sup>Although the exact value of  $\mathcal{L}_{\text{vol}}(\theta^*)$  is unknown, we can obtain an estimate by first performing a pre-training process using the linear combination loss. Based on this estimate, we can then adjust  $\epsilon_{\text{ub}}$  and  $\epsilon_{\text{lb}}$  accordingly.

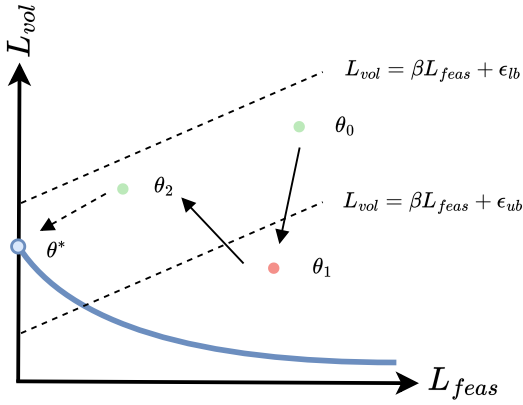


Fig. 2. The blue solid curve represents the Pareto front, while the black dashed lines indicate the upper and lower bounds. The green point denotes a feasible solution (i.e., a solution  $\theta$  with  $\mathbf{L}(\theta)$  lies between the two bounds), the red point represents an infeasible solution, and the blue point corresponds to  $\theta^*$ , the solution of problem 3. If the update causes  $\theta$  to fall outside the feasible region, the PCBF algorithm will gradually guide  $\theta$  back into the feasible region bounded by the upper and lower bounds.

All three subproblems are instances of problem (16) with  $M = 2$ . According to lemma 2, both losses will decrease as  $\theta_t$  approaches a Pareto critical solution. For subproblem (20), the update direction  $d_t$  reduces both  $\mathcal{L}_{\text{feas}}$  and  $\mathcal{L}_{\text{vol}} - \beta\mathcal{L}_{\text{feas}}$ , where the second term measures the violation of the upper bound. Once this violation decreases to be less than or equal to  $\epsilon_{\text{ub}}$ , the loss vector  $\mathbf{L}(\theta_t)$  returns to within the bounds. Similarly, subproblem (22) prevents  $\theta_t$  from violating the lower bound. For subproblem (21), the constraints incorporate both feasibility and volume losses. Following lemma 2, both losses decrease until a Pareto critical solution is reached.

To avoid  $\theta_t$  converging to a Pareto critical solution that is not Pareto optimal, a regularization term  $\gamma\mathcal{L}_{\text{vol}}$  is introduced, where  $\gamma$  is a small positive constant. This term serves two purposes: preventing convergence to a suboptimal Pareto critical solution and accelerating the training process. The pseudocode of the PCBF algorithm is shown in Algorithm 1, where analytical solutions for all subproblems are provided; for the proof, please refer to the Appendix.

#### IV. EXPERIMENTS

In this section, we evaluate the performance of the PCBF algorithm. First, we use a 2D inverted pendulum example, where the low dimensionality allows HJ Reachability to compute the infinite-time viability kernel as the ground truth for the largest inner safe set. Comparing PCBF results with HJ validates its effectiveness. Next, we extend to a 12-dimensional quadrotor obstacle avoidance scenario and run simulations to assess PCBF's performance in this more complex setting. Neural CBFs trained with linear combination loss (LCCBF) serve as our baseline. All neural networks are trained until convergence and share the same architecture (3 layers with 512, 256, 128 neurons and tanh activations).

---

#### Algorithm 1 Pareto Control Barrier Function (PCBF)

---

**Require:** Initial parameter  $\theta_0$ , learning rate  $\eta$ , hyperparameters  $\beta$ ,  $\epsilon_{\text{ub}}$ ,  $\epsilon_{\text{lb}}$ , regularization weight  $\gamma$ , max iterations  $T_{\text{max}}$ , initialization iterations  $T_{\text{init}}$ , convergence threshold  $\epsilon$ , initial state  $x_e$ , covariance matrix  $\Sigma$  used for Gaussian sampling.

**Ensure:** Optimal parameter  $\theta^*$

```

1:  $t \leftarrow 0$ ,  $\theta_t \leftarrow \theta_0$ 
2: // Gaussian sampling around  $x_e$ 
3:  $\mathbb{X}_{\mathcal{N}} \sim \mathcal{N}(x_e, \Sigma)$ 
4: // Initialization Phase
5: for  $t = 0$  to  $T_{\text{init}}$  do
6:    $\theta_{t+1} \leftarrow \theta_t - \eta(\lambda_1 \nabla \mathcal{L}_{\text{feas}}(\theta_t) + \lambda_2 \nabla \mathcal{L}_{\text{vol}}(\theta_t))$ 
7: end for
8: // Parameter Update Phase
9: for  $t = T_{\text{init}}$  to  $T_{\text{max}}$  do
10:  if  $\mathcal{L}_{\text{vol}}(\theta_t) > \beta\mathcal{L}_{\text{feas}}(\theta_t) + \epsilon_{\text{ub}}$  then
11:     $\lambda \leftarrow \max\left(\min\left(\frac{((1+\beta)\nabla\mathcal{L}_{\text{feas}}(\theta_t) - \nabla\mathcal{L}_{\text{vol}}(\theta_t))^T}{\|((1+\beta)\nabla\mathcal{L}_{\text{feas}}(\theta_t) - \nabla\mathcal{L}_{\text{vol}}(\theta_t))\|_2^2}, \nabla\mathcal{L}_{\text{feas}}(\theta_t), 1\right), 0\right)$ 
12:     $d_t \leftarrow (\lambda + \lambda\beta - 1)\nabla\mathcal{L}_{\text{feas}}(\theta_t) - \lambda\nabla\mathcal{L}_{\text{vol}}(\theta_t)$ 
13:  else if  $\beta\mathcal{L}_{\text{feas}}(\theta_t) + \epsilon_{\text{lb}} \leq \mathcal{L}_{\text{vol}}(\theta_t) \leq \beta\mathcal{L}_{\text{feas}}(\theta_t) + \epsilon_{\text{ub}}$ 
14:  then
15:     $\lambda \leftarrow \max\left(\min\left(\frac{(\nabla\mathcal{L}_{\text{feas}}(\theta_t) - \nabla\mathcal{L}_{\text{vol}}(\theta_t))^T \nabla\mathcal{L}_{\text{feas}}(\theta_t)}{\|\nabla\mathcal{L}_{\text{vol}}(\theta_t) - \nabla\mathcal{L}_{\text{feas}}(\theta_t)\|_2^2}, 1\right), 0\right)$ 
16:     $d_t \leftarrow -\lambda\nabla\mathcal{L}_{\text{vol}}(\theta_t) - (1 - \lambda)\nabla\mathcal{L}_{\text{feas}}(\theta_t)$ 
17:  else
18:     $\lambda \leftarrow \max\left(\min\left(\frac{(\nabla\mathcal{L}_{\text{vol}}(\theta_t) + (1-\beta)\nabla\mathcal{L}_{\text{feas}}(\theta_t))^T}{\|\nabla\mathcal{L}_{\text{vol}}(\theta_t) + (1-\beta)\nabla\mathcal{L}_{\text{feas}}(\theta_t)\|_2^2}, \nabla\mathcal{L}_{\text{feas}}(\theta_t), 1\right), 0\right)$ 
19:     $d_t \leftarrow (\lambda - \lambda\beta - 1)\nabla\mathcal{L}_{\text{feas}}(\theta_t) + \lambda\nabla\mathcal{L}_{\text{vol}}(\theta_t)$ 
20:  end if
21:   $\theta_{t+1} \leftarrow \theta_t + \eta(d_t - \gamma\nabla\mathcal{L}_{\text{vol}}(\theta_t))$ 
22:  if  $\|d_t\| < \epsilon$  or  $t = T_{\text{max}}$  then
23:    break
24:  end if
25: end for
26: return  $\theta_t$  as  $\theta^*$ 

```

---

#### A. Inverted Pendulum

The inverted pendulum dynamics are  $\dot{\theta} = \omega$ ,  $\dot{\omega} = \sin(\theta) + u$ , where  $\theta$  is the angle of the pendulum from the upright position,  $\omega$  is the angular velocity and  $u$  is the control input. The safe set is defined as  $|\theta| \leq \frac{\pi}{3}$ , and the input constraint is  $|u| \leq 1$ .

The left subfigure of Figure 3 shows a strong overlap between the inner safe set generated by PCBF and the infinite-time viability kernel from HJ reachability. Almost all states in the PCBF inner safe set fall within the viability kernel, demonstrating that PCBF effectively maximizes the safe set while ensuring safety. In contrast, the LCCBF-generated set shows significant discrepancies, with many states outside the kernel, leading to potential safety violations in practice.

We visualized the training process of PCBF and LCCBF in the right subfigure in Figure 3. Initially, LCCBF effectively approximates the boundary of the largest inner safe set,

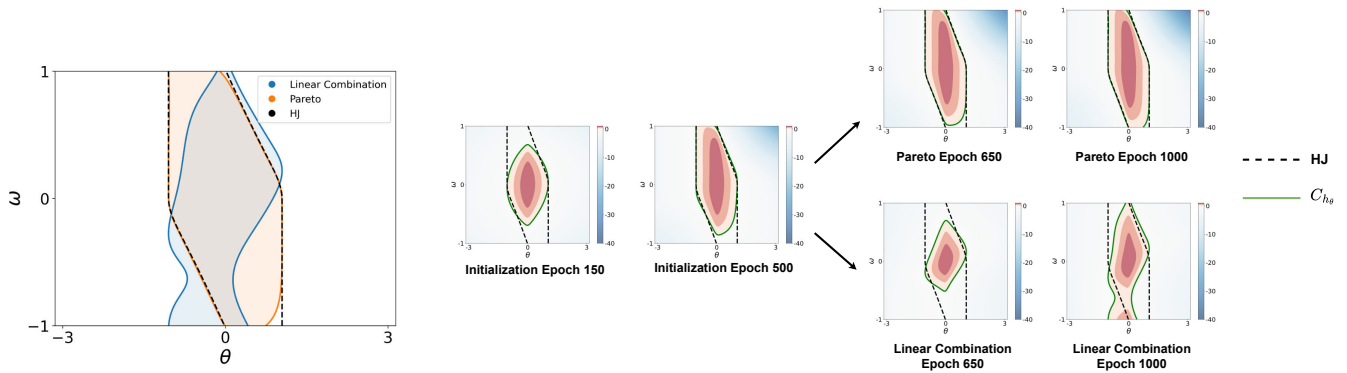


Fig. 3. The left subfigure visualizes the inner safe sets obtained by the LCCBF (blue solid line) and PCBF (orange solid line) methods, alongside the infinite-time viability kernel (black dashed line) computed using HJ reachability. The region enclosed by the black dashed line represents the true safe states. The right subfigure depicts the evolution of the inner safe sets (green solid lines) for both PCBF and LCCBF methods throughout the training process. During the initialization phase, both methods yield identical results as they both employ the linear combination loss initially.

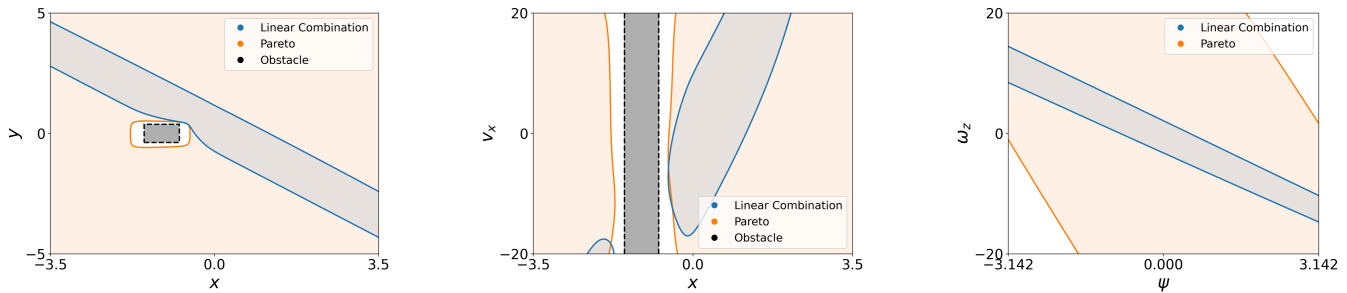


Fig. 4. The left, middle, and right subfigures present 2D slices of the learned inner safe sets obtained by the PCBF and ICCBF methods corresponding to the  $x - y$ ,  $x - v_x$ , and  $\psi - \omega_z$  planes. All other states are set to zero in each slice. In the left and middle subfigures, the obstacle's projection in the corresponding 2D plane is indicated by black dashed lines, representing regions unsafe for the quadrotor.

showing that the linear combination loss quickly captures the safe region's shape. However, as training progresses, LCCBF becomes unstable, with the learned inner safe set fluctuating unpredictably and failing to converge. In contrast, PCBF shows steady improvement as the volume of the learned safe set consistently growing

We also present the training times for different methods in Table I. In the sampling method column, "Boundary" refers to the sampling approach used in [6], while "Gaussian" represents the method proposed in this study. The results demonstrate a significant improvement in training efficiency with our new approach.

Model	Sampling Method	Sampling Num	Training Time (s)
LCCBF	Boundary	10000	17823 $\pm$ 713
LCCBF	Gaussian	10000	<b>1143 <math>\pm</math> 58</b>
PCBF	Boundary	10000	18356 $\pm$ 847
PCBF	Gaussian	10000	<b>1207 <math>\pm</math> 69</b>

TABLE I

TRAINING TIME FOR DIFFERENT SAMPLING METHODS ON NVIDIA GEFORCE RTX 3080TI

## B. Quadrotor

The state of the quadrotor involves its position  $x, y, z$ , velocity  $v_x, v_y, v_z$ , Euler angles  $\phi, \theta, \psi$ , and angular velocity  $\omega_x, \omega_y, \omega_z$ . The state dimension is 12 and the control dimension is 4. The system dynamics and input constraint can be found in [20]. A rectangular obstacle is placed in the scenario and the safe set is defined such that the quadrotor must maintain a minimum distance from the obstacle. Specifically, the safe set is  $x \leq -1.5$  or  $x \geq -0.75$  or  $y \leq -0.375$  or  $y \geq 0.375$ .

Figure 4 illustrates the inner safe sets of PCBF and LCCBF in various dimensions through 2D slices. Notably, the PCBF consistently yields a significantly larger inner safe set slice compared to the LCCBF across all slices. For example, in the left subfigure in Figure 4, where all states except  $x$  and  $y$  are set to zero, the quadrotor can hover in any unobstructed region. Consequently, the area outside the black region is safe. The inner safe set of the PCBF encompasses a substantial portion of the safe state, while the LCCBF's inner safe set is confined to a relatively small area. The volume of the inner safe set for the LCCBF is only 14% of that for the PCBF in the entire 12-dimensional state space.

We conducted simulations using RotorPy [21] in a windless environment with a refresh rate of 300 Hz. The nominal policy is based on the control algorithm proposed by [22].

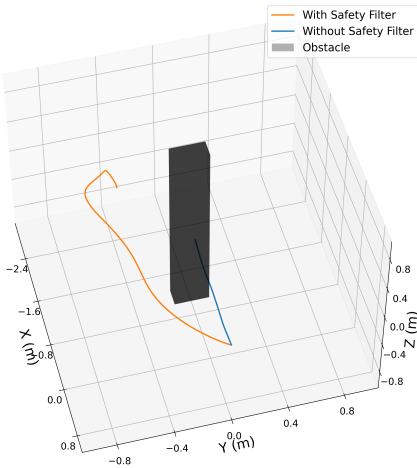


Fig. 5. Trajectories of the quadrotor with and without the PCBF safety filter in the presence of a rectangle obstacle.

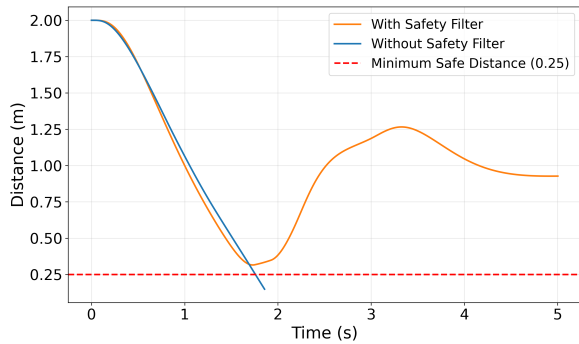


Fig. 6. Minimum distance to the rectangle obstacle with and without the PCBF safety filter.

When the PCBF safety filter is activated, we solve the CBF-QP problem 2 to derive a safe control policy. Figure 5 illustrates the simulation results, highlighting the quadrotor trajectories with and without the PCBF safety filter. The trajectory without the safety filter collides with an obstacle, while the trajectory using the safety filter successfully avoids it.

Figure 6 presents the minimum distance between the quadrotor and the rectangular obstacle over time, comparing the scenarios with and without the safety filter. The red dashed line represents the minimum safe distance of 0.25 meters. When the safety filter is not applied, the quadrotor approaches the obstacle dangerously close, breaching the minimum safe distance. In contrast, with the safety filter enabled, the quadrotor maintains a safe distance throughout the simulation.

## V. CONCLUSIONS

In this paper, we introduce the Pareto Control Barrier Function (PCBF) framework to maximize the inner safe set under input constraints. Using a Pareto multi-task learning approach, we balanced safety and set size, with PCBF significantly outperforming LCCBF methods. Comparisons with

HJ reachability for the inverted pendulum showed that PCBF closely approximates the largest inner safe set. Simulations with the quadrotor system further demonstrated PCBF's effectiveness in complex, high-dimensional environments. Future work will focus on adapting the PCBF framework to handle uncertainties in system dynamics and external disturbances.

## APPENDIX

### A. Proof of lemma 3

Let  $\theta^*$  be the solution to problem 3. Suppose  $\theta^*$  is not Pareto optimal. Then there exists a Pareto optimal  $\hat{\theta}$  such that:

$$\mathcal{L}_{\text{feas}}(\hat{\theta}) \leq \mathcal{L}_{\text{feas}}(\theta^*) = 0 \quad (23)$$

$$\mathcal{L}_{\text{vol}}(\hat{\theta}) \leq \mathcal{L}_{\text{vol}}(\theta^*) \quad (24)$$

with at least one of the inequalities being strict. However, since  $\mathcal{L}_{\text{feas}}(\theta^*) = 0$ , we must have  $\mathcal{L}_{\text{feas}}(\hat{\theta}) = 0$  as well. This means  $\hat{\theta}$  is also a feasible solution to problem 3. If  $\mathcal{L}_{\text{vol}}(\hat{\theta}) < \mathcal{L}_{\text{vol}}(\theta^*)$ , then  $\hat{\theta}$  would be a better solution to problem 3 than  $\theta^*$ , which contradicts the assumption that  $\theta^*$  is the solution to this problem. If  $\mathcal{L}_{\text{vol}}(\hat{\theta}) = \mathcal{L}_{\text{vol}}(\theta^*)$ , then  $\hat{\theta}$  is also an optimal solution to problem 3, and thus satisfies the conditions of the lemma.

Therefore, our assumption must be false, and  $\theta^*$  is indeed Pareto optimal. By definition,  $[\mathcal{L}_{\text{feas}}(\theta^*), \mathcal{L}_{\text{vol}}(\theta^*)]^T$  must lie on the Pareto front.

### B. Analytical solution for PCBF subproblems

Subproblems (20), (21), and (22) are special cases of problem (16) with  $M = 2$ . We first provide the general solution for problem (16). For  $M = 2$ , the problem becomes:

$$\begin{aligned} (d_t, \alpha_t) = \arg \min_{d \in \mathbb{R}^p, \alpha \in \mathbb{R}} \quad & \alpha + \frac{1}{2} \|d\|^2 \\ \text{s.t.} \quad & \nabla \mathcal{L}_1(\theta_t)^T d \leq \alpha \\ & \nabla \mathcal{L}_2(\theta_t)^T d \leq \alpha \end{aligned} \quad (25)$$

As problem (25) is a QP problem, we can apply the KKT conditions:

$$d_t + \lambda_1 \nabla \mathcal{L}_1(\theta_t) + \lambda_2 \nabla \mathcal{L}_2(\theta_t) = 0 \quad (26)$$

$$1 - \lambda_1 - \lambda_2 = 0 \quad (27)$$

$$\lambda_1 (\nabla \mathcal{L}_1(\theta_t)^T d_t - \alpha_t) = 0 \quad (28)$$

$$\lambda_2 (\nabla \mathcal{L}_2(\theta_t)^T d_t - \alpha_t) = 0 \quad (29)$$

$$\lambda_1, \lambda_2 \geq 0 \quad (30)$$

$$\nabla \mathcal{L}_1(\theta_t)^T d_t - \alpha_t \leq 0 \quad (31)$$

$$\nabla \mathcal{L}_2(\theta_t)^T d_t - \alpha_t \leq 0 \quad (32)$$

From the first two conditions, we get:

$$d_t = -\lambda_1 \nabla \mathcal{L}_1(\theta_t) - \lambda_2 \nabla \mathcal{L}_2(\theta_t) \quad (33)$$

$$\lambda_1 + \lambda_2 = 1 \quad (34)$$

Let  $\lambda_1 = \lambda$  and  $\lambda_2 = 1 - \lambda$ . Then:

$$d_t = -\lambda \nabla \mathcal{L}_1(\theta_t) - (1 - \lambda) \nabla \mathcal{L}_2(\theta_t) \quad (35)$$

To find  $\lambda$ , we use the complementary slackness conditions:

$$\lambda(\nabla\mathcal{L}_1(\theta_t)^T d_t - \alpha_t) = 0 \quad (36)$$

$$(1 - \lambda)(\nabla\mathcal{L}_2(\theta_t)^T d_t - \alpha_t) = 0 \quad (37)$$

This leads to three cases:

- If  $0 < \lambda < 1$ , then  $\nabla\mathcal{L}_1(\theta_t)^T d_t = \nabla\mathcal{L}_2(\theta_t)^T d_t = \alpha_t$   
Substituting  $d_t$  and solving for  $\lambda$ :

$$-\lambda\|\nabla\mathcal{L}_1(\theta_t)\|^2 - (1 - \lambda)\nabla\mathcal{L}_1(\theta_t)^T \nabla\mathcal{L}_2(\theta_t) \quad (38)$$

$$= -\lambda\nabla\mathcal{L}_2(\theta_t)^T \nabla\mathcal{L}_1(\theta_t) - (1 - \lambda)\|\nabla\mathcal{L}_2(\theta_t)\|^2$$

$$\lambda = \frac{(\nabla\mathcal{L}_2(\theta_t) - \nabla\mathcal{L}_1(\theta_t))^T \nabla\mathcal{L}_2(\theta_t)}{\|\nabla\mathcal{L}_1(\theta_t) - \nabla\mathcal{L}_2(\theta_t)\|_2^2} \quad (39)$$

- If  $\lambda = 0$ , then  $\nabla\mathcal{L}_2(\theta_t)^T d_t = \alpha_t$  and  $\nabla\mathcal{L}_1(\theta_t)^T d_t \leq \alpha_t$
- If  $\lambda = 1$ , then  $\nabla\mathcal{L}_1(\theta_t)^T d_t = \alpha_t$  and  $\nabla\mathcal{L}_2(\theta_t)^T d_t \leq \alpha_t$

Combining these conditions leads to the following solution:

$$\lambda = \max\left(\min\left(\frac{(\nabla\mathcal{L}_2(\theta_t) - \nabla\mathcal{L}_1(\theta_t))^T \nabla\mathcal{L}_2(\theta_t)}{\|\nabla\mathcal{L}_1(\theta_t) - \nabla\mathcal{L}_2(\theta_t)\|_2^2}, 1\right), 0\right) \quad (40)$$

Replacing  $\mathcal{L}_1$  and  $\mathcal{L}_2$  with specific losses in problems (20), (21), and (22) leads to the following analytical solutions:

- 1) If  $\mathcal{L}_{\text{vol}}(\theta_t) > \beta\mathcal{L}_{\text{feas}}(\theta_t) + \epsilon_{\text{ub}}$ :

$$d_t = (\lambda + \lambda\beta - 1)\nabla\mathcal{L}_{\text{feas}}(\theta_t) - \lambda\nabla\mathcal{L}_{\text{vol}}(\theta_t) \quad (41)$$

where

$$\lambda = \max\left(\min\left(\frac{((1 + \beta)\nabla\mathcal{L}_{\text{feas}}(\theta_t) - \nabla\mathcal{L}_{\text{vol}}(\theta_t))^T}{\|(1 + \beta)\nabla\mathcal{L}_{\text{feas}}(\theta_t) - \nabla\mathcal{L}_{\text{vol}}(\theta_t)\|_2^2} \cdot \nabla\mathcal{L}_{\text{feas}}(\theta_t), 1\right), 0\right) \quad (42)$$

- 2) If  $\beta\mathcal{L}_{\text{feas}}(\theta_t) + \epsilon_{\text{lb}} \leq \mathcal{L}_{\text{vol}}(\theta_t) \leq \beta\mathcal{L}_{\text{feas}}(\theta_t) + \epsilon_{\text{ub}}$ :

$$d_t = -\lambda\nabla\mathcal{L}_{\text{vol}}(\theta_t) - (1 - \lambda)\nabla\mathcal{L}_{\text{feas}}(\theta_t) \quad (43)$$

where

$$\lambda = \max\left(\min\left(\frac{(\nabla\mathcal{L}_{\text{feas}}(\theta_t) - \nabla\mathcal{L}_{\text{vol}}(\theta_t))^T \nabla\mathcal{L}_{\text{feas}}(\theta_t)}{\|\nabla\mathcal{L}_{\text{vol}}(\theta_t) - \nabla\mathcal{L}_{\text{feas}}(\theta_t)\|_2^2}, 1\right), 0\right) \quad (44)$$

- 3) If  $\mathcal{L}_{\text{vol}}(\theta_t) < \beta\mathcal{L}_{\text{feas}}(\theta_t) + \epsilon_{\text{lb}}$ :

$$d_t = (\lambda - \lambda\beta - 1)\nabla\mathcal{L}_{\text{feas}}(\theta_t) + \lambda\nabla\mathcal{L}_{\text{vol}}(\theta_t) \quad (45)$$

where

$$\lambda = \max\left(\min\left(\frac{(\nabla\mathcal{L}_{\text{vol}}(\theta_t) + (1 - \beta)\nabla\mathcal{L}_{\text{feas}}(\theta_t))^T}{\|\nabla\mathcal{L}_{\text{vol}}(\theta_t) + (1 - \beta)\nabla\mathcal{L}_{\text{feas}}(\theta_t)\|_2^2} \cdot \nabla\mathcal{L}_{\text{feas}}(\theta_t), 1\right), 0\right) \quad (46)$$

## REFERENCES

- [1] A. D. Ames, S. Coogan, M. Egerstedt, G. Notomista, K. Sreenath, and P. Tabuada, "Control barrier functions: Theory and applications," in *2019 18th European Control Conference (ECC)*. IEEE, 2019, pp. 3420–3431.
- [2] Q. Nguyen and K. Sreenath, "Safety-critical control for dynamical bipedal walking with precise footstep placement," *IFAC-PapersOnLine*, vol. 48, no. 27, pp. 147–154, 2015.
- [3] A. Alan, A. J. Taylor, C. R. He, A. D. Ames, and G. Orosz, "Control barrier functions and input-to-state safety with application to automated vehicles," *IEEE Transactions on Control Systems Technology*, vol. 31, no. 6, pp. 2744–2759, 2023.
- [4] D. R. Agrawal and D. Panagou, "Safe control synthesis via input constrained control barrier functions," in *2021 60th IEEE Conference on Decision and Control (CDC)*. IEEE, 2021, pp. 6113–6118.
- [5] J. Breeden and D. Panagou, "High relative degree control barrier functions under input constraints," in *2021 60th IEEE Conference on Decision and Control (CDC)*. IEEE, 2021, pp. 6119–6124.
- [6] S. Liu, C. Liu, and J. Dolan, "Safe control under input limits with neural control barrier functions," in *Conference on Robot Learning*. PMLR, 2023, pp. 1970–1980.
- [7] O. So, Z. Serlin, M. Mann, J. Gonzales, K. Rutledge, N. Roy, and C. Fan, "How to train your neural control barrier function: Learning safety filters for complex input-constrained systems," in *2024 IEEE International Conference on Robotics and Automation (ICRA)*. IEEE, 2024, pp. 11 532–11 539.
- [8] L. Lindemann and D. V. Dimarogonas, "Control barrier functions for signal temporal logic tasks," *IEEE control systems letters*, vol. 3, no. 1, pp. 96–101, 2018.
- [9] B. Xu and K. Sreenath, "Safe teleoperation of dynamic uavs through control barrier functions," in *2018 IEEE International Conference on Robotics and Automation (ICRA)*. IEEE, 2018, pp. 7848–7855.
- [10] C. Dawson, S. Gao, and C. Fan, "Safe control with learned certificates: A survey of neural Lyapunov, barrier, and contraction methods for robotics and control," *IEEE Transactions on Robotics*, vol. 39, no. 3, pp. 1749–1767, 2023.
- [11] S. M. Richards, F. Berkenkamp, and A. Krause, "The Lyapunov neural network: Adaptive stability certification for safe learning of dynamical systems," in *Conference on Robot Learning*. PMLR, 2018, pp. 466–476.
- [12] J. Z. Kolter and G. Manek, "Learning stable deep dynamics models," *Advances in neural information processing systems*, vol. 32, 2019.
- [13] W. Xiao, T.-H. Wang, R. Hasani, M. Chahine, A. Amini, X. Li, and D. Rus, "Barriernet: Differentiable control barrier functions for learning of safe robot control," *IEEE Transactions on Robotics*, vol. 39, no. 3, pp. 2289–2307, 2023.
- [14] I. M. Mitchell, A. M. Bayen, and C. J. Tomlin, "A time-dependent hamilton-jacobi formulation of reachable sets for continuous dynamic games," *IEEE Transactions on automatic control*, vol. 50, no. 7, pp. 947–957, 2005.
- [15] J. J. Choi, D. Lee, K. Sreenath, C. J. Tomlin, and S. L. Herbert, "Robust control barrier–value functions for safety-critical control," in *2021 60th IEEE Conference on Decision and Control (CDC)*. IEEE, 2021, pp. 6814–6821.
- [16] K. Garg, S. Zhang, O. So, C. Dawson, and C. Fan, "Learning safe control for multi-robot systems: Methods, verification, and open challenges," *Annual Reviews in Control*, vol. 57, p. 100948, 2024.
- [17] E. Zitzler and L. Thiele, "Multiobjective evolutionary algorithms: A comparative case study and the strength pareto approach," *IEEE transactions on Evolutionary Computation*, vol. 3, no. 4, pp. 257–271, 1999.
- [18] S. Boyd and L. Vandenberghe, *Convex optimization*. Cambridge university press, 2004.
- [19] J. Fliege and B. F. Svaiter, "Steepest descent methods for multicriteria optimization," *Mathematical methods of operations research*, vol. 51, pp. 479–494, 2000.
- [20] R. W. Beard, "Quadrotor dynamics and control," *Brigham Young University*, vol. 19, no. 3, pp. 46–56, 2008.
- [21] S. Folk, J. Paulos, and V. Kumar, "Rotorpy: A python-based multi-robot simulator with aerodynamics for education and research," *arXiv preprint arXiv:2306.04485*, 2023.
- [22] T. Lee, M. Leok, and N. H. McClamroch, "Geometric tracking control of a quadrotor uav on se (3)," in *49th IEEE conference on decision and control (CDC)*. IEEE, 2010, pp. 5420–5425.